

K^- - p Interactions from 594 to 820 MeV/ c

L. BERTANZA, A. BIGI, R. CARRARA, R. CASALI, AND R. PAZZI

Istituto di Fisica dell' Università-Pisa, Istituto Nazionale di Fisica Nucleare. Sezione di Pisa

AND

D. BERLEY, E. L. HART,* D. C. RAHM, W. J. WILLIS† AND S. S. YAMAMOTO‡

Brookhaven National Laboratory,§ Upton, New York 11973

AND

N. S. WONG

Yale University,§ New Haven, Connecticut 06520

(Received 25 July 1968)

K^- - p interactions in the Columbia-BNL 30-in. hydrogen bubble chamber were studied at nine momenta from 594 to 820 MeV/ c . The results for elastic-scattering and zero-prong-plus- V^0 events are presented here. Differential cross sections are given for the K^-p , \bar{K}^0n , and $\Delta\pi^0$ final states. A fit to the $\bar{K}N$ channels was obtained which shows the effects of a $\frac{3}{2}^-$ resonance at 1701 MeV. This energy is appreciably displaced from the peak in the inelastic cross section.

I. INTRODUCTION

THIS paper presents part of the results of a survey of K^- - p reactions in the momentum region 594–820 MeV/ c . The reactions reported here are elastic scattering and those which give rise to a disappearing K^- and a single V^0 . The reactions leading to charged Σ hyperons and to two-pronged interactions and a V^0 will be presented separately. Preliminary results on all the reactions have been published.^{1–3}

The range of c.m. energies covered is 1605–1710 MeV. This is the appropriate quantity for the masses of hyperon resonances appearing in “formation” or in s channel, as shown in Fig. 1. The upper limit of mass of a resonance which can be “produced,” with an additional pion, as in Fig. 2, ranges from 1470 to 1575 MeV/ c^2 . At the time this experiment was undertaken the only known resonance capable of appearing in the s channel was the $\Sigma(1660)$ (that is, a hyperon with isospin 1 and mass 1660 MeV/ c^2), which should be seen at a K^- momentum of 715 ± 24 MeV/ c . Indeed, its effects had been reported in an earlier experiment,⁴ studying K^- - p interactions at 620, 760, and 850 MeV/ c .

In the course of the experiment, we have found that the actual situation is much more complicated. The

coupling of the $\Sigma(1660)$ to the $\bar{K}N$ channel is certainly rather small; as described in Sec. V, it could be of the order of 0.03.

Our first result concerned the reaction $K^- + p \rightarrow \Lambda + \pi^0$, which had been reported⁵ to show the effects of the $\Sigma(1660)$ and to give a spin-parity result of $\frac{3}{2}^+$. We found a small admixture of $\Sigma(1660)$, with a $\frac{5}{2}^-$ background amplitude which increased rapidly with energy. This is now known to be due to the $\Sigma(1770)$ which occurs at higher energy, though it had not then been established. The analysis¹ somewhat favored spin-parity $\frac{3}{2}^-$, a result which is now generally accepted.⁶ In this paper, we describe the technique used to obtain the final $\Lambda\pi^0$ data.

Meanwhile, we found an unexpected resonance at 1675 MeV, most prominent in the $K^-p \rightarrow \Lambda\eta$ channel, with $J^P = \frac{1}{2}^-$; and another $T=0$ resonance, $\Lambda(1690)$, with spin and parity $\frac{3}{2}^-$ has been discovered,^{3,7,8} helping to explain certain features of our data. Another resonance, $\Sigma(1690)$, has been seen in production, but

⁵ M. Taher-Zadeh, D. Prowse, P. Schlein, W. Slater, D. Stork, and H. Ticho, Phys. Rev. Letters **11**, 470 (1963).

⁶ P. Eberhard, M. Pripstein, F. Shively, O. Kruse, and R. Swanson, Phys. Rev. **163**, 1446 (1967); G. London, R. Rau, N. Samios, S. Yamamoto, M. Goldberg, S. Lichtman, M. Primer, and J. Leitner, *ibid.* **143**, 1034 (1966); Y. Lee, D. Reeder, and R. Hartung, Phys. Rev. Letters **17**, 45 (1966); P. Schlein and T. Trippe, University of California Report No. UCLA-1016, 1966 (unpublished); this paper reanalyzes the data of Ref. 5 and favors $\frac{3}{2}^-$. On the other hand, results favoring $\frac{3}{2}^+$ are found by A. Leveque, M. Ville, P. Negus, W. Blair, A. Grant, I. Hughes, R. Turnbull, A. Ahmad, S. Baker, L. Celnikier, S. Misbahuddin, I. Skillicorn, J. Loken, R. Sekulin, J. Mulvey, A. Atherton, G. Chadwick, W. Davies, J. Field, P. Gray, D. Lawrence, L. Lyons, A. Oxley, C. Wilkinson, C. Fisher, E. Pickup, L. Rangan, J. Scarr, and A. Segar, Phys. Letters **18**, 69 (1965).

⁷ R. Armenteros, M. Ferro-Luzzi, D. Leith, R. Levi-Setti, A. Minten, R. Tripp, H. Filthuth, V. Hepp, E. Kluge, H. Schneider, R. Barloutaud, P. Granet, J. Meyer, and J. Porte, Phys. Letters **24B**, 198 (1967); see also Ref. 3.

⁸ J. Davies, J. Dowell, P. Hattersley, R. Homer, A. O'Dell, A. Carter, K. Riley, R. Tapper, D. Bugg, R. Gilmore, K. Knight, D. Salter, G. Stafford, and E. Wilson, Phys. Rev. Letters **18**, 62 (1967).

* Present address: University of California, Riverside, Calif.

† Present address: Yale University, New Haven, Conn.

‡ Present address: University of Massachusetts, Amherst, Mass.

§ Research performed under the auspices of the U. S. Atomic Energy Commission.

¹ D. Berley, P. Connolly, E. Hart, D. Rahm, D. Stonehill, B. Thevenet, W. Willis, and S. Yamamoto, in *Proceedings of the International Conference on High-Energy Physics at Dubna, 1964* (Atomizdat, Moscow, 1966), Vol. I, p. 565.

² D. Berley, P. Connolly, E. Hart, D. Rahm, D. Stonehill, B. Thevenet, W. Willis, and S. Yamamoto, Phys. Rev. Letters **15**, 641 (1965); **16**, 162 (E) (1966).

³ D. Rahm *et al.*, in *Proceedings of the Thirteenth Annual International Conference on High-Energy Physics, Berkeley, 1966* (University of California Press, Berkeley, 1967), in Report by M. Ferro-Luzzi, p. 201.

⁴ P. Bastien and J. P. Berge, Phys. Rev. Letters **10**, 188 (1963).

apparently has little coupling to the $\bar{K}N$ channel.⁹ The complicated structure in this energy region, reviewed recently in Ref. 10, has been predicted on the basis of the quark model.¹¹

It is the aim of this paper to describe the methods used in obtaining the differential and partial cross sections, and to offer tentative interpretations of the phenomena observed. It is our belief that increased statistical accuracy will be necessary to achieve a definitive analysis.

II. BEAM AND BUBBLE CHAMBER

The secondary beam was taken at 22° to a target in the Brookhaven A. G. S. The beam, which was designed for another purpose (to provide stopping \bar{p} and K^-), proved adequate for the present experiment, providing six K^- with a few times 10¹⁰ protons on the target. One stage of electrostatic mass separation was used, employing a standard 15-ft separator, giving a $K^- : \pi^- : \mu^-$ ratio of 1:1:1. The pion background constitutes an analysis problem only for elastic scattering, since the pion energy is below the threshold for associated production of strange particles.

The momentum acceptance of the beam was approximately triangular with an ideal width of about 1%, at half-maximum. The K^- momentum was varied by tuning the beam, except for the 594-MeV/c point, where a carbon degrader was used, with the beam tuned for 650 MeV/c.

The detector was the Columbia-Brookhaven 30-in. hydrogen bubble chamber, which has a magnetic field of about 13 kG.

III. ELASTIC SCATTERING

In order to analyze the elastic events we undertook to scan and measure about 25 000 pictures at 708, 725, 741, 768, and 802 MeV/c. All two- and three-prong events found in a restricted fiducial region and a sample of one-prong events were measured on image plane digitizers and analyzed on the Pisa IBM 7090 computer. Part of the measurements were monitored by an on-line computer (CEP). Because of the approximately 30% π^- -contamination of the beam, mentioned above, it was necessary to allow for the fact that very forward $\pi-p$ and $K-p$ elastic scattering are essentially indistinguishable. Since a good separation based on the

⁹ M. Derrick, T. Fields, J. Loken, R. Ammar, R. Davis, W. Kropac, J. Mott, and F. Schweingruber, *Phys. Rev. Letters* **18**, 266 (1967); D. Colley, F. MacDonald, B. Musgrave, W. Blair, I. Hughes, R. Turnbull, S. Goldsack, K. Paler, L. Sisterson, W. Blum, W. Allison, D. Locke, L. Lyons, P. Finney, C. Fisher, and A. Segar, *Phys. Letters* **24B**, 489 (1967).

¹⁰ These complications are discussed by J. Meyer, in *Proceedings of the Heidelberg International Conference on Elementary Particles*, edited by H. Filthuth (Interscience Publishers, Inc., New York, 1968), p. 117.

¹¹ R. Dalitz, in *Proceedings of the Oxford International Conference on Elementary Particles, 1965* (Rutherford High-Energy Laboratory, Chilton, Berkshire, England, 1966).

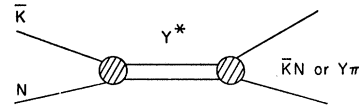


FIG. 1. Schematic representation of the observation of a resonance in an S channel, or formation, experiment.

kinematic analysis and ionization estimates was found possible for events with $\cos\theta^* < 0.8$ (θ^* being the c.m. system scattering angle of the meson), only these events were accepted. With this cutoff, azimuth angle distributions were found to be isotropic.

The quality of the separation between π and K events was tested by comparison of our $\pi^- - p$ differential distributions with counter results^{12,13} at nearby energies (Fig. 3), and good agreement was found. The normalization was chosen in order to obtain the same integrated cross sections in the overlap region $-1 < \cos\theta^* < 0.6$.

To obtain the K^- path length, we counted the one-prong events in the fiducial region in all scanned frames. About 800 of them at each momentum were measured and a correction for off-beam tracks was derived, using acceptance criteria consistent with those used for elastic events. Moreover, azimuth losses were determined for different decay angles Φ . Events with $\Phi < 10^\circ$ (i.e., about 10% of all one-prong K decays, all the $\pi - \mu$ decays, and possible elastic events with very short recoil) were removed from the sample, and a correction was calculated, taking into account the known branching ratios for the various K -decay modes. Furthermore, small, angle-independent scanning efficiency corrections were made to all data.

In Fig. 4 the corrected differential cross sections are shown. The points at $\cos\theta^* = 1$ were obtained from the total $K^- - p$ cross section in Table IV, and the dispersion relation calculations by Holley *et al.*¹⁴ The data points (including the 0° point) were fitted to Legendre poly-

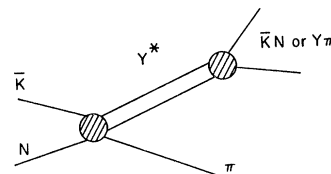


FIG. 2. Schematic representation of the observation of a resonance in a production experiment.

¹² J. Helland, C. Wood, T. Devlin, D. Hagge, M. Longo, B. Moyer, and V. Perez-Mendez, *Phys. Rev.* **134**, B1079 (1964).

¹³ P. Odgen, D. Hagge, J. Helland, M. Banner, J. Detoeuf, and J. Teiger, *Phys. Rev.* **137**, B1115 (1965).

¹⁴ W. Holley, E. Beall, D. Keefe, L. Kerth, J. Thresher, C. Wang, and W. Wenzel, Lawrence Radiation Laboratory Report No. UCRL-16875, 1966 (unpublished). The dispersion-relation calculation for Ref(0) will not reflect the effects of nearby resonances which were not adequately resolved in the total cross sections used. We can calculate the real part due to the $\Delta(1690)$ with $X=0.25$, which will give the largest effect. We obtain $|\text{Re}f(0)|^2 = 0.13$. To allow for this effect, we have doubled the errors on $|\text{Re}f(0)|^2$ given in this reference.

TABLE I. Elastic scattering.

P_{K^-} (MeV/c)	No. of events	$ \text{Im}f(0) ^2$	$ \text{Re}f(0) ^2$	a_0	a_1	a_2	a_3	a_4	σ_{K^-p} (mb)
708	432	2.62 ± 0.25	0.36 ± 0.18	1.76 ± 0.12	2.37 ± 0.22	1.19 ± 0.21	0.10 ± 0.21	-0.26 ± 0.19	13.5 ± 0.9
725	604	2.92 ± 0.23	0.44 ± 0.22	1.57 ± 0.10	2.22 ± 0.21	1.63 ± 0.23	0.48 ± 0.21	0.15 ± 0.18	11.5 ± 0.8
741	341	2.72 ± 0.22	0.50 ± 0.25	1.65 ± 0.11	2.29 ± 0.20	1.90 ± 0.20	0.23 ± 0.17	-0.05 ± 0.18	11.6 ± 0.7
768	417	4.44 ± 0.40	0.62 ± 0.31	2.27 ± 0.15	3.31 ± 0.28	3.17 ± 0.30	1.15 ± 0.24	0.14 ± 0.22	15.2 ± 1.0
802	866	5.16 ± 0.43	0.78 ± 0.39	3.10 ± 0.20	4.23 ± 0.42	4.25 ± 0.49	1.05 ± 0.41	0.29 ± 0.37	19.3 ± 1.3

nomial series of the form

$$d\sigma/d\Omega = (1/4k^2) \sum_l a_l P_l(\cos\theta^*). \quad (1)$$

A fourth-order fit was found to be satisfactory at all momenta. The corresponding values of the coefficients a_l are plotted in Fig. 13, and listed in Table I, together with the other pertinent data. In Fig. 5, the total elastic cross sections, as obtained by integration under the fitted differential curves, are given along with the measurements available in the region of incident momentum $700 < P_K < 900$ MeV/c.^{14,15,21}

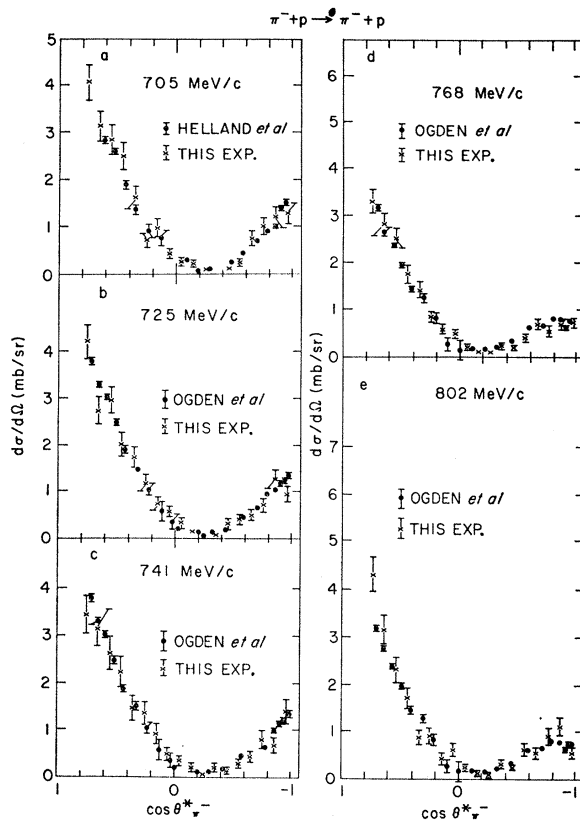


FIG. 3. Comparison of the π^-p elastic-scattering angular distribution obtained in this experiment with the results of counter experiments.

¹⁵ N. Gelfand, D. Harmsen, R. Levi-Setti, E. Predazzi, M. Raymund, J. Doede, and W. Männer, Phys. Rev. Letters **17**, 1224 (1966).

IV. V^0 ANALYSIS PROCEDURES

A. Scanning

The scanners recorded any V^0 inside a fiducial region, any one-prong decay into a meson which stopped in the chamber, and any three-pronged decay of a beam track. (The scan for charged Σ^\pm decays was made at the same time, but will not be described in this paper.) The three-pronged decays are largely τ decays into $\pi^-\pi^-\pi^+$, but also include other decay modes with a Dalitz electron pair.

A partial rescanning of the film gave single scan efficiencies of $(96 \pm 1)\%$ for V^0 's and $(94 \pm 1)\%$ for the three-prong decays.

B. Geometry and Kinematics

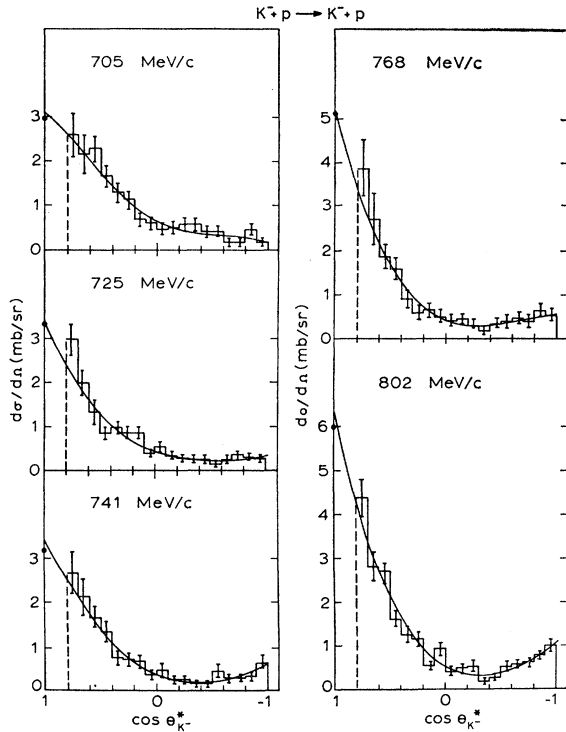
Geometrical reconstruction from measurements made in the two best views for each track was carried out by TRED programs as modified by H. Yuta to take into account all three components of the magnetic field. The version of KICK due to Kopp¹⁶ was used for kinematic analysis. First, a three-constraint fit was made to the V^0 , assuming it to originate at a point one mean bubble gap length past the measured endpoint of the beam track. If this fit failed, a one-constraint fit was made without a measured direction for the neutral particle. The fits were made for the decays $\bar{K}^0 \rightarrow \pi^+\pi^-$ and $\Lambda \rightarrow p^+\pi^-$. If the decay fit succeeded, a one-constraint fit was made to the production reaction.

C. Beam Energy

The average energy of the K^- beam for each of the nine runs was determined by several methods. The most accurate depended on the kinematics of the reaction $K^- + p \rightarrow \Lambda + \eta$. Near the threshold, at 725 MeV/c, the momentum and angle of the Λ are very sensitive to the momentum of the K^- . The momenta of the runs at 725, 741, 768, and 802 MeV/c were thereby determined in a way which is insensitive to the calibration of the magnetic field or systematic distortions.

Another method used the range and decay angle of muons from decays $K^- \rightarrow \mu^- + \nu$ with the muon stopping in the bubble chamber. These events yield an accurate measurement, largely independent of systematic effects.

¹⁶ J. Kopp, Kick Manual, Brookhaven Bubble Chamber Group Internal Report (unpublished).

FIG. 4. Differential cross section for K^-p elastic scattering.

The range of the muon tends to be too long to stop at the lower end of our momentum range, and too short at the upper end so that these momenta were not as well determined.

These measurements were in good agreement with each other, and with the values from the fitted K^- momenta of highly constrained events. Comparison with beam track measurement indicated that the magnetic field was about 0.99 times the nominal value.

The values adopted are given in Table II. The systematic errors on these values should be less than 1% for 594 and 820 MeV/c and less than $\frac{1}{2}$ % for the other momenta.

D. Event Identification

The output of the kinematic calculation was processed by another computer program which assigned events to the various reactions, if this could be done by kinematics alone. The logic proceeded as follows.

The V^0 fits were examined to see if the Λ and \bar{K}^0 interpretations, from the measured origin, were allowed. (An interpretation was accepted if the χ^2 was less than six times the number of constraints.) If neither V^0 fit from the measured origin was acceptable, the one-constraint fits were printed out, with a flag which indicated that the event needed further treatment.

If both Λ and \bar{K}^0 fits were possible the event was flagged as ambiguous, and temporarily assigned as a \bar{K}^0+n reaction if the production fit was good, and

otherwise as a Λ . These ambiguities could almost always be resolved by visual bubble-density estimates. It was found that ambiguous V^0 's which failed the \bar{K}^0+n fit were almost all Λ 's, but those which made the fit contained comparable fractions of \bar{K}^0 and Λ 's and had to be individually inspected.

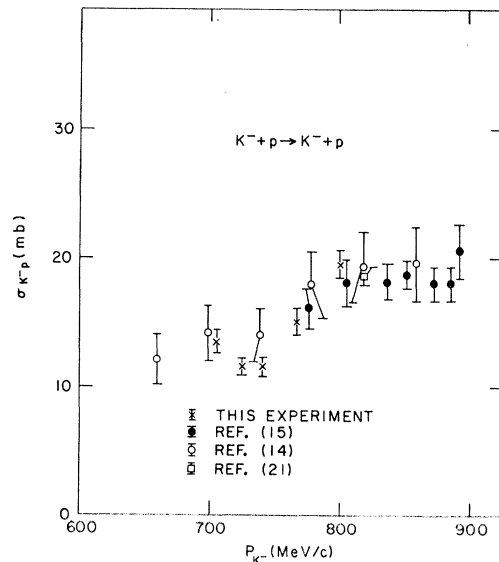
If the V^0 had an unambiguous fit to a \bar{K}^0 , the one-constraint production fit and the missing mass were examined, and the event assigned to the \bar{K}^0+n or $\bar{K}^0+n+\pi^0$ reactions, or to a "no-production fit" category which received very few events (3% of the \bar{K}^0). There was almost no ambiguity between the charge-exchange reactions and those with the production of an extra π^0 .

If the V^0 had a fit as a Λ , a fit to $K^-+p \rightarrow \Lambda+\pi^0$ was attempted. The primary analysis of the Λ reactions is based on the missing-mass distribution, however. Since this analysis involves the angular distribution, it will be discussed in Sec. IV G.

E. Cross-Section Normalization

The number of three-prong K^- decays was used to normalize the cross sections, in a way which needs no correction for K^- attenuation due to interactions and decays. The decay length for these decays was computed from the K^- lifetime and the branching ratio for decay into three prongs. An inspection by a physicist checked the scanners' claim that a three-prong event was really a K decay.

The fraction of three-prong decays which met the criteria set for beam tracks was determined by measuring a sample of about two-thirds of the events at each energy. This fraction of the recorded number of decays times the computed decay length gave the K^- path length at each energy.

FIG. 5. K^-p elastic-scattering cross section.

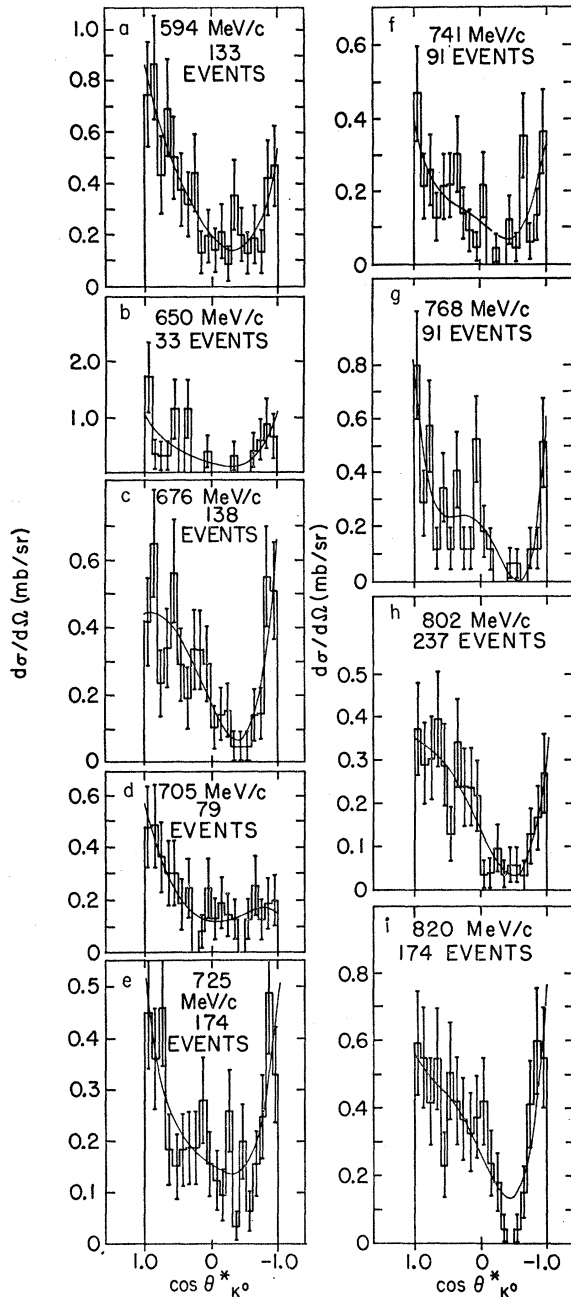


FIG. 6. Differential cross section for K^-p charge-exchange scattering.

After one remeasurement, 1% of the V^0 's did not make a three-constraint fit. It was found that about half of these were real V^0 's associated with an origin in the chamber, and the cross sections were increased accordingly. A similar adjustment was made for the unambiguous \bar{K}^0 's with no production fit.

F. \bar{K}^0 Results

Two angle-dependent corrections must be made to the observed \bar{K}^0 events. First, there is a loss of events

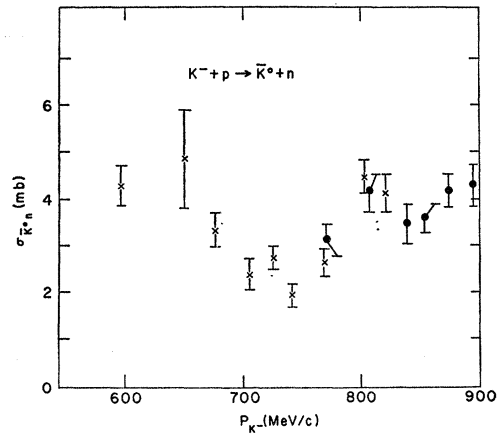


FIG. 7. Cross section for K^-p charge-exchange scattering.

which decay before traveling the minimum acceptable distance, the "length cutoff," or live long enough to escape from the V^0 fiducial volume before decaying. (The former loss is much the more important.) Second, there is a scanning loss when the opening angle of the \bar{K}^0 in the laboratory is near 180° , so that the V^0 looks like a background track traversing the chamber with a slight kink. Both losses are greater for slow \bar{K}^0 's, and consequently for charge-exchange events where the \bar{K}^0 emerges at a large angle. The former correction could be calculated accurately, but it was considered best to determine the latter empirically.

The loss of large opening angle \bar{K}^0 's was investigated by means of histograms of the cosine of the decay angle between the \bar{K}^0 line of flight and the π^+ momentum, in the \bar{K}^0 rest frame. This distribution should be uniform, but the scanning loss leads to a dip for decay angles near 90° , allowing the loss to be estimated. This was done as a function of the production angle of the \bar{K}^0 . The correction was found to be rather small, ranging from 0 to 7%.

To correct for the neutral decays of the \bar{K}^0 , the observed number of events was multiplied by the factor given by the $\Delta I = \frac{1}{2}$ rule, $\frac{3}{2}$.

The corrected histograms showing the angular distributions in the K^-p rest frame are shown in Fig. 6. The charge-exchange cross section as a function of energy appears in Table II and is shown in Fig. 7.

The differential cross sections were fit to Legendre polynomials with the normalization

$$\frac{d\sigma}{d\Omega} = \left(\frac{1}{4k^2}\right) \sum_l a_l P_l(\cos\theta). \quad (1)$$

The coefficients a_l were evaluated by forming the moments of $P_l(\cos\theta)$ averaged over the sample of N events, giving each event a weight inversely proportional to the product of the two detection factors discussed above:

$$M_l = \frac{\sum_{i=1}^N w_i P_l(\cos\theta_i)}{\sum_{i=1}^N w_i}. \quad (2)$$

TABLE II. Charge-exchange cross section.

P_{K^-} (MeV/c)	$\sigma_{K^0 n}$ (mb)	a_0	a_1	a_2	a_3	a_4	a_5
594	4.40 ± 0.44	0.45 ± 0.05	0.29 ± 0.09	0.41 ± 0.12	-0.08 ± 0.13	0.04 ± 0.15	-0.20 ± 0.18
650	5.0 ± 1.1	0.58 ± 0.12	0.19 ± 0.25	0.79 ± 0.35	-0.26 ± 0.38	0.18 ± 0.43	0.83 ± 0.51
668	3.47 ± 0.34	0.42 ± 0.04	0.17 ± 0.08	0.34 ± 0.11	-0.33 ± 0.12	0.07 ± 0.13	0.05 ± 0.15
708	2.56 ± 0.33	0.34 ± 0.04	0.21 ± 0.09	0.26 ± 0.11	0.12 ± 0.12	-0.02 ± 0.14	-0.03 ± 0.15
725	2.90 ± 0.25	0.40 ± 0.03	0.07 ± 0.07	0.35 ± 0.09	-0.05 ± 0.10	0.11 ± 0.12	0.09 ± 0.14
741	2.09 ± 0.25	0.30 ± 0.04	0.10 ± 0.07	0.28 ± 0.10	-0.10 ± 0.11	0.14 ± 0.13	0.11 ± 0.15
768	2.79 ± 0.33	0.42 ± 0.05	0.32 ± 0.10	0.41 ± 0.14	-0.11 ± 0.16	0.48 ± 0.19	0.10 ± 0.20
802	4.68 ± 0.37	0.75 ± 0.05	0.55 ± 0.11	0.47 ± 0.14	-0.51 ± 0.17	0.17 ± 0.19	0.05 ± 0.20
820	4.35 ± 0.39	0.72 ± 0.06	0.24 ± 0.12	0.46 ± 0.16	-0.43 ± 0.17	0.19 ± 0.20	0.25 ± 0.22

Since the Legendre polynomials are orthogonal, division of the moments by a normalization factor gives an estimate of the coefficients,

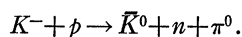
$$a_l = (2l+1)M_l a_0 \quad (3)$$

with

$$a_0 = (k^2/\pi)\sigma_{K^0 n}.$$

The variance matrix of the a_l is diagonal, to a fair approximation, in this case.¹⁷ The τ -based normalization described in Sec. IV E is used to obtain the normalized a_l coefficients as defined in Eq. (1), which are presented in Table II, and Figure 14, with the errors increased by the statistical error on the number of three-pronged decays.

The events with an identified \bar{K}^0 and a missing mass greater than that of a neutron plus a π^0 are assumed to be examples of



Although these events are not kinematically constrained, no background subtraction seemed to be required, judging from the paucity of events with missing masses above the neutron peak but below the $n + \pi^0$

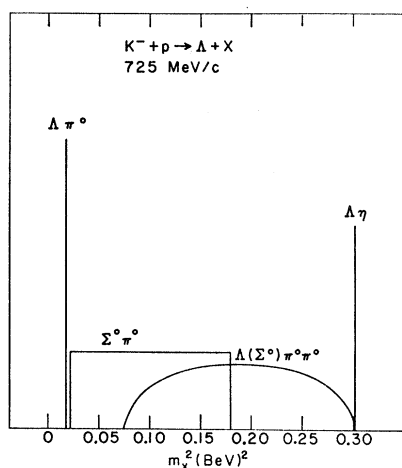


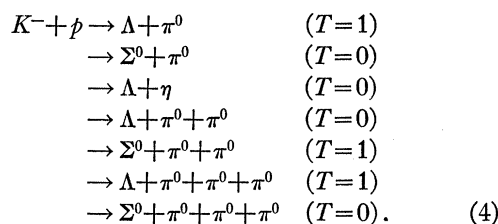
FIG. 8. Form of the distribution of missing-mass squared which would be observed in the reaction $K^- + p \rightarrow \Lambda + \text{neutrals}$ with perfect resolution.

¹⁷ R. Glasser, quoted by R. Uhlig, thesis, University of Maryland Technical Report No. 545, 1966 (unpublished).

threshold. The cross section for these events appears in Table IV.

G. Results on Λ Reactions

The problem here is to assign the events among the multitude of reactions which can give rise to a Λ plus neutrals:



Only the $\Lambda\pi^0$ and $\Lambda\eta$ reactions offer any kinematic constraints, but some further information may be gained by considering the missing-mass distribution, which is linearly related to the energy of the observed Λ . The idealized distribution for perfect resolution is shown in Fig. 8 for a P_{K^-} of 725 MeV/c. (The upper limit of the missing-mass distribution for $\Sigma^0\pi^0$, as well as for the multipion reactions, is a function of K^- momentum.) A measured distribution is shown in Fig. 9.

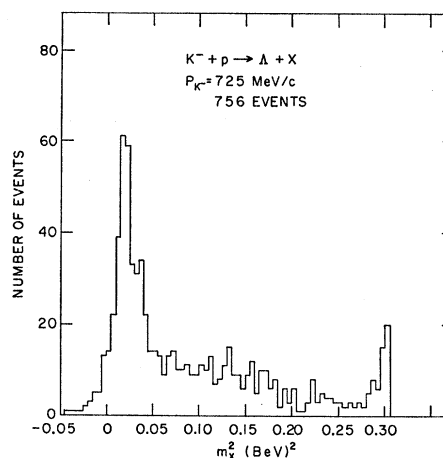


FIG. 9. Missing-mass-squared distribution with fitted Λ 's from $K^- p$ interactions at 725 MeV/c.

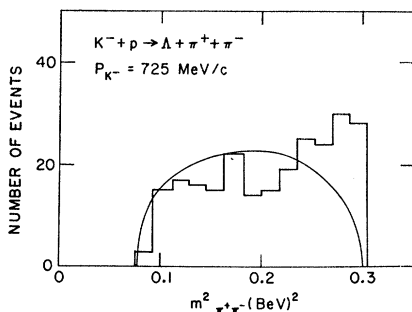


FIG. 10. Pion-pion mass-squared distribution in the reaction $K^-p \rightarrow \Lambda\pi^+\pi^-$ at 725 MeV/c. The deviation from the phase-space distribution shows that the phase-space distributions should not be relied upon in the case of two neutral pions, Fig. 8 and 9.

If one may judge from the $\Lambda\pi^+\pi^-\pi^0$ reaction, omitting $\Lambda\eta$ events, the number of events involving three pions is very small, except possibly at 820 MeV/c, and these were ignored in the subsequent analysis.

It is not likely that the missing-mass distributions in the two-pion reactions conform to the result of a phase-space calculation ignoring final-state interactions. In fact, a guide to the expected distributions *might* be found in corresponding results for the well-identified reaction leading to $\Lambda\pi^+\pi^-$. An example, for 725 MeV/c, is shown in Fig. 10. It shows two-pion effective masses, corresponding to the missing-mass distribution in the $\Lambda\pi^0\pi^0$ case, which peak near the upper end, with little resemblance to the shape of phase space. However, the comparison is probably not valid. The peak in Fig. 10 is apparently due to the interference of the decays of $\Sigma^\pm(1385)$ in a $T=1$ state.¹ Such a state is *forbidden* for $\Lambda\pi^0\pi^0$. The major contribution to the two- π^0 reactions may well come from the $\Sigma^0\pi^0\pi^0$ reactions, involving $\Lambda(1405)$ production, but there are similar difficulties in relating it to the analyzable reactions $\Sigma^0\pi^+\pi^-$ and $\Sigma^\pm\pi^\mp\pi^0$. In conclusion, the missing-mass distributions corresponding to the two- π^0 reactions cannot be predicted at this time.

In view of these considerations, it seems unwise to obtain the $\Sigma^0\pi^0$ cross section by making an over-all fit to the missing-mass distribution assuming phase-space distributions for the multipion reactions, though this has been done in some experiments and yields relatively small statistical errors. We have attempted to perform analyses which give reasonable upper and lower limits on the number of $\Sigma^0\pi^0$ events.

The information contained in the Λ distributions is of two types, afflicted by different uncertainties, and it is convenient to treat them separately. First, there is the portion of the missing-mass distribution below the mass of two π^0 's, including the $\Lambda\pi^0$ and about one-third of the $\Sigma^0\pi^0$ events. The problem here is to know the resolution function so that these categories may be separated. The region with missing masses larger than two π^0 's can be used if the shapes of the two-pion distributions are assumed, by normalizing them to the

region beyond the $\Sigma^0\pi^0$ limit, excluding the $\Lambda\eta$ region. The former method seems to offer more promise in principle, and will be considered first.

The resolution function was obtained by generating a Gaussian distribution with the width given by KICK as the error of missing-mass squared for each event, and adding these distributions for events in intervals of K^- energy and Λ angle. It was found that the over-all distribution is *not* at all a Gaussian, but at a *given* Λ angle the distribution is nearly Gaussian. Also, the width of the resolution function is a strong function of Λ angle. A satisfactory characterization of the resolution function was then obtained by fitting a Gaussian, with a width written as a power series in the Λ angle, to the resolution functions generated from the real events. This fit does seem to give curves in agreement with the shape of the Λ peak, at different angles.

A method of analysis has been devised which does not require that an individual event be assigned as a $\Lambda\pi^0$ or a $\Sigma^0\pi^0$, and reflects the uncertainty of the $\Lambda\pi^0$ angular distribution Legendre series coefficients a_i^Λ , due to the $\Sigma^0\pi^0$ background. This is a moment calculation where the function used is not just P_i , but P_i times the missing-mass distribution function, evaluated for each event. There are two such functions, one for $\Lambda\pi^0$ and one for $\Sigma^0\pi^0$, obtained by folding the distributions shown in Fig. 8 with the experimental resolution function whose determination was described in the previous paragraph. Thus one computes two moments for each P_i , one for $\Lambda\pi^0$ and one for $\Sigma^0\pi^0$. If the missing-mass distributions for these two reactions did not overlap, these would reduce to the ordinary moments of P_i . Since there is some overlap, the two sets of moments will be coupled, and it is necessary to solve a set of $2L$ simultaneous equations relating the moments to the estimates of a_i^Λ and a_i^Σ , where $L-1$ is the maximum order of P_i taken into account. The coefficients in these

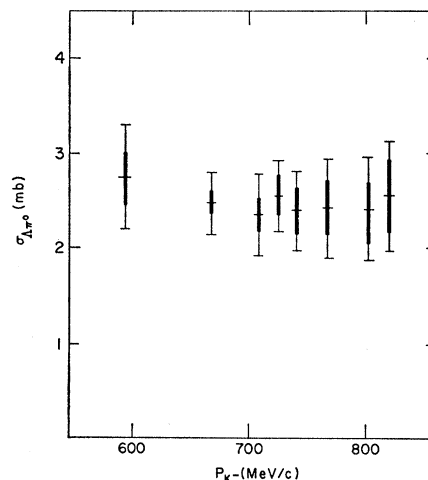


FIG. 11. Cross section for $K^-+p \rightarrow \Lambda+\pi^0$, showing limits for systematic errors, as described in the text, as heavy bars, with the statistical errors added to these limits.

equations are obtained by numerical integration of the products of the distribution functions, according to the usual method of moments. More exactly, the moments are defined by

$$M_i^Y = \frac{\sum_{i=1}^N P_i(\cos\theta_i) w_i f^Y(y_i, \cos\theta_i)}{\sum_{i=1}^N w_i}, \quad (5)$$

where Y may be Λ or Σ^0 , the quantity f is the value of the computed distribution function for the event, y_i is equal to the missing mass squared, and w_i is the weight. The weight included the corrections for the loss of decays near the point of production and outside the fiducial volume, as for the \bar{K}^0 's, and a small correction for the loss of Λ 's with short protons, revealed by plotting the proton direction in the Λ frame for different intervals in Λ production angle. The coefficients of the equations relating the M_i^Y with the a_i^Y are, with $x = \cos\theta$,

$$C_{l,m}^{YY'} = \int \int dx dy P_l(x) P_m(x) f^Y(y,x) f^{Y'}(y,x). \quad (6)$$

The function $f^{\Sigma^0}(y,x)$ was generated by folding the ideal $\Sigma^0\pi^0$ distribution with the resolution function, which was assumed to be independent of y over this rather small range of missing masses. The $C_{l,m}^{YY'}$ were evaluated numerically. Then, in terms of $2L$ -dimensional matrices, the expression for the Legendre coefficient is

$$\mathbf{a} = \mathbf{C}^{-1}\mathbf{M}.$$

This method essentially uses the expected missing-mass distributions as weights for computing " $\Lambda\pi^0$ moments" and " $\Sigma^0\pi^0$ moments." It is believed that this technique is not much inferior to a maximum-likelihood calculation which would be considerably more expensive in computer time. The computation was carried out for moments of P_l up to P_6 . The error matrix was most conveniently calculated by directly averaging the second moments over the sample:

$$\mathbf{V} = (1/N) \langle (\mathbf{a}_i - \mathbf{a})(\mathbf{a}_i - \mathbf{a})^T \rangle, \quad (7)$$

where \mathbf{a}_i is the estimate from an individual event, and T denotes the transpose. The resulting error matrix has large off-diagonal terms, which should be used in any further statistical calculations.

The missing-mass-squared distributions corresponding to the computed coefficients were generated and compared to the experimental plots as a check. They were indeed good fits over the region used, below the two- π^0 threshold.

In order to make use of the other source of information on the number of $\Sigma^0\pi^0$'s, the events above the two- π^0 mass, "extreme" assumptions about the distribution of the multipion events were made. An assumed distribution which peaks toward high pion-pion masses, will, when normalized to the region beyond the $\Sigma^0\pi^0$ endpoint, give a relatively low number of multipion

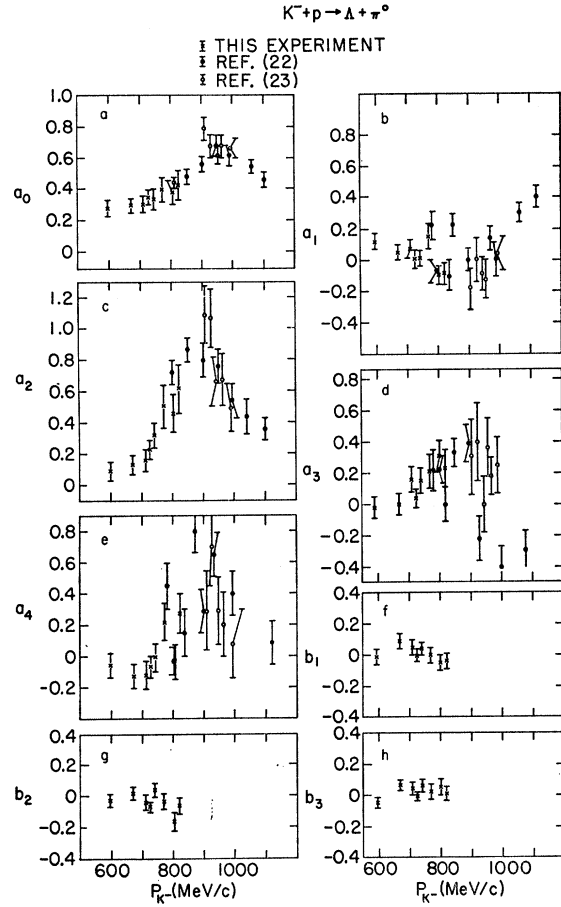


FIG. 12. Coefficients in the Legendre expansion of the $K^-p \rightarrow \Lambda\pi^0$ differential cross section.

events in the $\Sigma^0\pi^0$ region, and thus a relatively large estimate for the number of $\Sigma^0\pi^0$ events. Since it turned out that this assumption gave a somewhat *smaller* number than the estimate from events below the two- π^0 threshold, the range of the estimate reaches the more interesting limit for the other kind of distribution, peaked at low pion-pion masses.

A reasonable example of an extreme distribution in this regard was produced by using the mirror image of the experimental distribution for $\Lambda\pi^+\pi^-$, which peaks at high pion-pion masses. (The distribution for $\Sigma^0\pi^0\pi^0$ will be somewhat distorted by the decay of the Σ^0 to the observed Λ and a γ , but this effect can be neglected in view of our uncertainty about the original spectrum.)

The result of these two independent analyses is two values of the number of $\Sigma^0\pi^0$'s at each energy. The fact that the independent estimate from the moment analysis falls at one extreme of the range of values estimated from the events overlapping with the multipion reactions may be due to a systematic effect in the first method, such as insufficient knowledge of the resolution function, or may reflect the effect of a pion-pion distribution strongly peaked at high masses.

TABLE III. $\Lambda\pi^0$ angular distribution Legendre coefficients.*

P_{K^-} (MeV/c)	a_0	a_1	a_2	a_3	a_4	b_1	b_2	b_3
594	0.28 ± 0.05	0.12 ± 0.05	0.09 ± 0.06	-0.02 ± 0.07	-0.06 ± 0.08	-0.01 ± 0.05	-0.03 ± 0.04	-0.05 ± 0.03
668	0.30 ± 0.04	0.05 ± 0.05	0.13 ± 0.06	0.01 ± 0.07	-0.13 ± 0.08	0.09 ± 0.04	0.02 ± 0.04	0.06 ± 0.03
708	0.31 ± 0.05	0.07 ± 0.06	0.16 ± 0.07	0.16 ± 0.08	-0.12 ± 0.09	0.05 ± 0.05	-0.04 ± 0.05	0.04 ± 0.04
725	0.35 ± 0.05	-0.01 ± 0.04	0.23 ± 0.06	0.04 ± 0.06	-0.07 ± 0.07	0.00 ± 0.04	-0.07 ± 0.03	-0.01 ± 0.03
741	0.34 ± 0.06	0.01 ± 0.05	0.32 ± 0.08	0.15 ± 0.08	-0.01 ± 0.09	0.04 ± 0.04	0.04 ± 0.04	0.06 ± 0.04
768	0.36 ± 0.08	0.15 ± 0.08	0.51 ± 0.14	0.21 ± 0.11	0.22 ± 0.12	-0.01 ± 0.05	-0.03 ± 0.05	0.02 ± 0.05
802	0.38 ± 0.08	-0.10 ± 0.06	0.46 ± 0.12	0.26 ± 0.10	-0.03 ± 0.09	-0.05 ± 0.05	-0.17 ± 0.06	-0.05 ± 0.04
820	0.42 ± 0.09	-0.09 ± 0.07	0.62 ± 0.16	0.23 ± 0.11	0.27 ± 0.13	-0.04 ± 0.05	-0.06 ± 0.05	0.01 ± 0.04

* The systematic error shown in Fig. 11 is not included in these errors.

Our procedure has been to accept the values from the moment analysis and the multipion region as representing the probable extremes of the systematic error, choosing as the "best" estimate the upper limit from the second method, and to add, linearly, the statistical errors to obtain the error range for the $\Sigma^0\pi^0$ cross section. Since a known fraction of the $\Sigma^0\pi^0$ form a background in the $\Lambda\pi^0$ region, the two cross sections are somewhat related, and the $\Lambda\pi^0$ cross section is given a range of systematic uncertainty.

The angular distribution adopted is based on the moment analysis, but the transformation involved in normalizing a_0^A to the number of events in the "best" estimate is not, because of the nondiagonal error matrix, simply a multiplication by a factor. By a standard statistical procedure,¹⁸ if we change a_0^2 obtained in the moment analysis to $a_0^{2'}$, the most probable values of the coefficients are given by

$$\mathbf{a}_\Lambda' = \mathbf{a}_\Lambda + \mathbf{V}_{12}(\mathbf{V}_{22})^{-1}(\mathbf{a}_\Sigma' - \mathbf{a}_\Sigma), \quad (8)$$

where \mathbf{V}_{12} and \mathbf{V}_{22} are submatrices of the error matrix

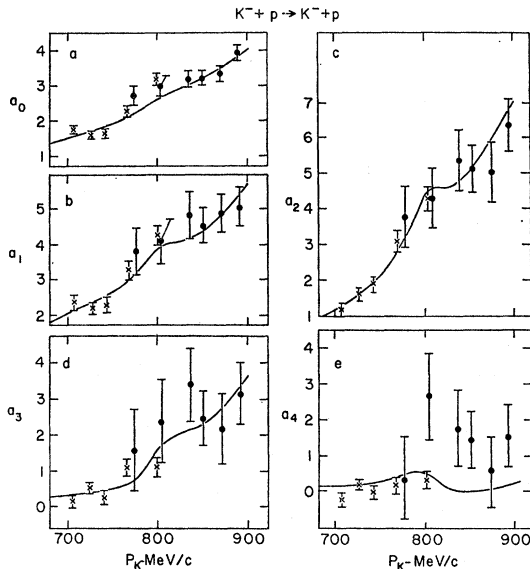


FIG. 13. Coefficients in the Legendre expansion of the K^-p elastic-scattering differential cross section.

¹⁸ A. Mood and F. Graybill, *Introduction to the Theory of Statistics* (McGraw-Hill Book Co., New York, 1963), p. 213.

\mathbf{V} defined in Eq. (7), partitioned according to the index Y .

The errors on the a_i^A are also transformed, by

$$\mathbf{V}_{11}' = \mathbf{V}_{11} - \mathbf{V}_{12}(\mathbf{V}_{22})^{-1}\mathbf{V}_{21}. \quad (9)$$

Finally the a_i^A are normalized by the use of the three-prong decays, and the errors suitably increased. $\sigma_{\Lambda\pi^0}$ is shown in Fig. 11 and the resulting a_i^A are given in Table III and in Fig. 12.

The cross sections for the $\Lambda\pi^0$, $\Sigma^0\pi^0$, and $(\Lambda$ or $\Sigma^0)\pi^0\pi^0$ reactions are given in Table IV, along with the cross sections for all the other observed processes (Fig. 16). The values for cross sections involving two-prong-plus- V^0 events are preliminary. The total cross sections can be compared with those of Davies *et al.*⁸ The agreement is good for the higher-momentum points, but for the lower-momentum points, 708, 725, and 741 MeV/c, we find cross sections which are lower by several standard deviations. We have not been able to find an energy-dependent bias in our normalization procedure. [Because of the optical-theorem contribution to the forward point, our elastic-scattering cross sections are

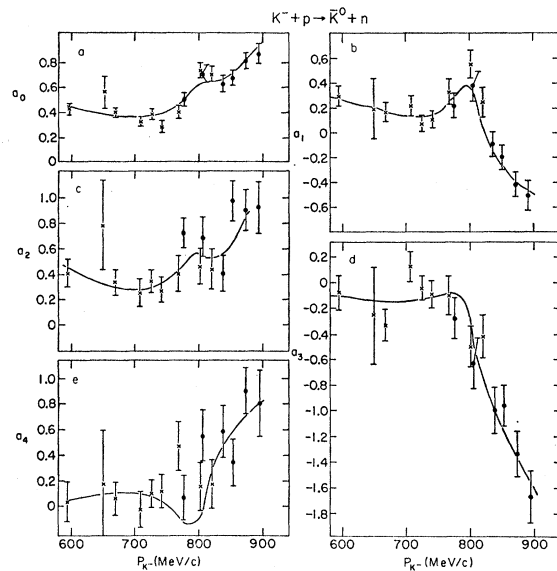


FIG. 14. Coefficients in the Legendre expansion of the K^-p charge-exchange differential cross section.

TABLE IV. Cross sections (in mb) for all the observed processes.

Channel \ P_{K^-} (MeV/c)	594	650	668	708	725	741	768	802	820
$\Lambda\pi^0$	2.78±0.55		2.51±0.33	2.38±0.42	2.56±0.36	2.43±0.38	2.46±0.52	2.43±0.52	2.58±0.56
$\Lambda\pi^+\pi^-$	2.1 ±0.3	2.3 ±0.5	2.20±0.4	3.00±0.35		3.19±0.3	3.64±0.3	3.97±0.3	3.26±0.35
$\Sigma^+\pi^-$	3.75±0.32	4.18±0.63	3.05±0.27	2.62±0.29	3.14±0.25	2.43±0.23	3.18±0.34	2.31±0.24	2.32±0.21
$\Sigma^-\pi^+$	2.54±0.23	2.93±0.46	2.91±0.25	3.77±0.35	4.69±0.30	4.42±0.34	4.23±0.39	2.24±0.19	2.59±0.20
$\Sigma^0\pi^+\pi^-$	0.14±0.08	0.28±0.18	0.37±0.15	0.45±0.18		0.55±0.10	0.80±0.13	0.61±0.17	0.60±0.15
$\Sigma^+\pi^-\pi^0$	0.23±0.06	0.53±0.18	0.25±0.06	0.41±0.09	0.76±0.09	0.67±0.10	0.79±0.13	0.67±0.09	0.89±0.10
$\Sigma^-\pi^+\pi^0$	0.32±0.07	0.41±0.13	0.32±0.06	0.38±0.07	0.65±0.07	0.64±0.09	0.85±0.12	0.65±0.08	0.87±0.09
$K^0\eta\pi^0$	0.0 ±0.1	0.15±0.15	0.07±0.04	0.12±0.06	0.08±0.03	0.15±0.06	0.06±0.04	0.29±0.07	0.26±0.08
$\Lambda\pi^0\pi^0$									
$\Sigma^0\pi^0\pi^0$									
$\Sigma^0\pi^0\pi^0$									
etc. ^b									
$\Lambda\pi^+\pi^-\pi^0$ ^b	0.0 ±0.06	0.0 ±0.1	0.0 ±0.05	0.0 ±0.06	0.08±0.03	0.32±0.08	0.32±0.07	0.14±0.05	0.10±0.04
Inelastic ^c	14.5 ±1.0		14.5 ±1.0	16.5 ±1.2	(18.9 ±1.0) ^d	18.2 ±1.0	20.5 ±1.4	16.2 ±1.0	16.6 ±1.0
$\bar{K}N$	16.1 ±1.0	14.4 ±0.7	13.7 ±0.8	18.0 ±1.1	24.0 ±1.1	23.1 ±0.8 ^e
Total	32.6 ±1.6	33.3 ±1.2	31.9 ±1.4	38.5 ±1.8	40.2 ±1.5	39.7 ±1.3
$\Sigma^0\pi^0$	1.7 ±1.0	...	1.5 ±0.5	2.0 ±0.7	1.9 ±0.7	1.7 ±0.7	2.4 ±0.5	1.0 ±0.9	1.3 ±1.0
$\Lambda\eta$	0	0	0	0	see Ref. 2	0.93±0.14	0.71±0.11	0.21±0.09	0.07±0.08

^a The $\Sigma^0\pi^0$ cross section is included. The estimate of this cross section alone, with a larger error is given below.

^b The $\Lambda\eta$ cross section is included here. The $\Lambda\eta$ cross section is given below from Ref. 2.

^c Correlations have been taken into account in computing the errors on these cross sections.

^d Missing partial cross sections interpolated.

^e With elastic scattering from L. Sodickson, I. Mannelli, D. Frisch, and M. Wahlig, Phys. Rev. 133, B757 (1964).

sensitive to the value used for the inelastic cross section. If the cross section of Davies *et al.* is adopted, the changes in the elastic-scattering cross section are +0.6 mb (708 MeV/c), +0.6 mb (725 MeV/c), +1.1 mb (741 MeV/c), -0.2 mb (768 MeV/c), and +0.1 mb (802 MeV/c.)

V. CONCLUSIONS

Since the results for the $\Lambda\pi^0$ and $\Lambda\eta$ reactions have been discussed in previous papers, we here concentrate on the elastic-scattering and charge-exchange reactions. Our object is to see if these can be interpreted in terms of the known resonances $\Sigma(1660)$, $\Lambda(1670)$, $\Lambda(1690)$, and $\Sigma(1770)$.

The most interesting structure in the $\bar{K}N$ reactions appears at momenta around 800 MeV/c. This is just at the upper end of our momentum region, and at the lower end of the CERN-Heidelberg-Saclay (CHS) run. The CHS collaboration has recently presented a partial-wave analysis of their charge-exchange data¹⁹ and of the elastic-scattering data obtained from the same exposure by the Chicago group,¹⁵ in the momentum band 780-1200 MeV/c.

As mentioned in the Introduction, this analysis suggests the presence of the $\Lambda(1690)$ with $J^P = \frac{3}{2}^-$ or D_{03} , in the notation $L_{I,2J}$. They find a resonant energy $E_R = 1699 \pm 2$ MeV, width $\Gamma = 33 \pm 15$ MeV, and elasticity $x = \Gamma_{el}/\Gamma = 0.19 \pm 0.07$. It was observed, however, that this resonance lies at the lower edge of the momentum region examined, so that no firm conclusion on its properties could be drawn. Their fit does not agree with our data below 800 MeV/c.

¹⁹ R. Armenteros, M. Ferro-Luzzi, D. Leith, R. Levi-Setti, A. Minten, R. Tripp, H. Filthuth, V. Hepp, E. Kluge, H. Schneider, R. Barloutaud, P. Granet, J. Meyer, and J. Porte, Phys. Letters 24B, 198 (1967).

Since our data cover the low side of the resonance, we thought it worthwhile to use the two sets of results for a new partial-wave fit in the region 600-900 MeV/c. We used the same assumptions as in the CHS work: The resonant amplitudes were described by a non-relativistic Breit-Wigner form, the background amplitudes were parametrized as linear functions of the laboratory momentum, and no background was assumed in the resonant partial waves.

The program MINUIT²⁰ was used to find the best fit to the data under the following conditions: (a) One, at most, of the amplitudes D_{03} , P_{03} , P_{01} is resonant in the 1700-MeV region. The parameters of the resonant amplitude are fit. (b) The D_{13} amplitude is resonant at 1662 MeV with $\Gamma = 49$ MeV. The elasticity is fixed at 0.03, or in some cases fit. (c) The other resonant amplitudes are kept fixed, with the CHS²¹ parameters. (d) The background amplitudes are fit. (No resonance is assumed in the S waves.) (e) Unitarity is imposed.

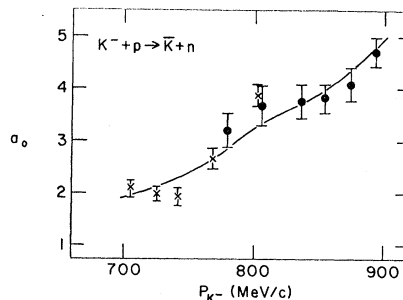


FIG. 15. The a_0 coefficient in the Legendre expansion of the $K^-p \rightarrow \bar{K}n$ differential cross section, the sum of the elastic and charge-exchange scattering.

²⁰ F. James and M. Roos, MINUIT, CERN Library D506, 1967 (unpublished).

²¹ R. Uhlig, G. Charlton, P. Condon, R. Glasser, G. Yodh, and N. Seeman, Phys. Rev. 155, 1448 (1967).

TABLE V. Results of fits to elastic and charge-exchange scattering.

$Y(1700)^a$ resonant state	χ^2/N_D	E_R , MeV	Γ , MeV	$x(1700)$	$x(1660)$	State	Background ^b			
							Rea	Ima	Reb	Imb
D_{03}	149/103	1701	28	0.28	0.03 fixed	S_{01}	0.20	0.79	0.19	0.77
						S_{11}	0.11	0.74	0.53	1.03
						P_{01}	-0.07	0.63	-0.66	0.78
						P_{11}	-0.10	0.05	-0.33	-0.29
						P_{03}	-0.21	0.52	-0.96	1.30
						P_{13}	-0.29	0.21	-0.20	0.25
P_{03}	180/103	1717	143	0.49	0.03 fixed	S_{01}	0.05	0.54	0.67	0.49
						S_{11}	-0.15	0.45	-0.57	1.55
						P_{01}	-0.02	1.08	0.95	2.04
						P_{11}	-0.08	0.58	0.33	1.12
						D_{03}	-0.07	-0.13	-0.09	-0.78
						P_{13}	-0.15	0.14	-0.87	-0.04
P_{01}	190/103	1699	38	0.43	0.03 fixed	S_{01}	-0.00	0.66	0.09	0.09
						S_{11}	0.49	0.55	1.99	1.23
						P_{11}	-0.04	-0.14	0.10	-0.43
						P_{03}	-0.19	0.72	-0.49	1.31
						P_{13}	-0.34	0.35	-0.56	0.34
						D_{03}	-0.26	0.07	-1.06	-0.06

^a Other resonant states parametrized as in the CHS work (Ref. 19).

^b The background amplitudes are parametrized by $a+b(P_{K^-}-1)$, where P_{K^-} is the laboratory momentum in GeV/c.

The results are shown in Table V. The best fit so far obtained under these assumptions corresponds to a D_{03} partial wave resonant at 1701 ± 4 MeV, with $\Gamma = 28 \pm 8$ MeV and elasticity $x = 0.28 \pm 0.04$, where the errors indicated have only a qualitative significance. The elasticity of the $\Sigma(1660)$ was fixed at 0.03, a value at which it has an ill-defined minimum in some fits. The fits are not sensitive to this parameter. This fit is shown in Figs. 13 and 14. It is very similar to the CHS fit at the upper end of the momentum interval.

The χ^2 of this fit is 149 for 103 degrees of freedom. The fit is improbable statistically, but it does reproduce the general shape of the experimental points rather well. There does seem to be a discrepancy in the comparison with the a_0 coefficients for K^-p and \bar{K}^0n . These show a more pronounced peak at 800 MeV/c than the fitted

curve does. This is more evident in the plot of $a_0^{KN} = a_0^{K^-p} + a_0^{\bar{K}^0n}$, Fig. 15. The interference term between $T=0$ and $T=1$ isotopic spin states vanishes in this sum. This kind of discrepancy might be evidence for a failure of the assumption that there is no background in the resonant partial wave.

Another peculiarity worth noting is that the energy of the D_{03} resonance, presumably to be identified with the $\Lambda(1690)$, is determined to be 1701 MeV from this fit to the $\bar{K}N$ channels, but was found to be 1682 MeV in the fit to the $\Sigma\pi$ channels.⁷ The data for these fits came from the same bubble-chamber exposures, so there can be no question of energy calibration. The inelastic cross section, excluding \bar{K}^0n , from this experiment is given in Table IV and in Fig. 16. There is a peak around 750 MeV/c due to unresolved contributions from $\Sigma(1660)$, $\Lambda(1670)$, and $\Lambda(1690)$. The largest contribution is probably from $\Lambda(1690)$. The inelastic peak, which comes largely but not entirely from the $\Sigma\pi$ reactions, is seen to lie around 1680 MeV, removed from the 1701-MeV value by at least one half-width. The peak in the total $T=0$ cross sections was found by Davies *et al.*⁸ to be at 1700 MeV.

The shift between the elastic and inelastic resonant energies seems to be a real effect. The width obtained here for the D_{03} resonance, 24 MeV, is also rather inconsistent with that found in the $\Sigma\pi$ channels, 55 MeV. Perhaps it is due to a channel shift of a single resonance, or it may indicate a more complicated structure than has been assumed.

Fits were also tried for a P_{01} or P_{03} resonance, with poorer χ^2 , as shown in Table V. A fit assuming no resonance around 1700 MeV gave a χ^2 of 202 for 102 degrees of freedom.

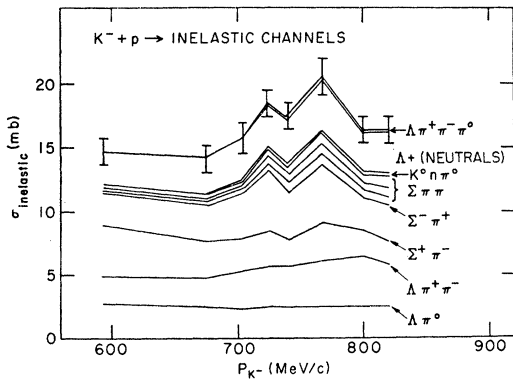


FIG. 16. Inelastic cross section excluding charge-exchange scattering, as a function of K^- momentum. The composition by individual channels is shown. (The $K^-p \rightarrow K^0p\pi^-$ channel is not shown. On the basis of very few events, this cross section was found to be less than 0.1 mb at all momenta.)

Even within the assumptions made in searching for a partial-wave fit, the present results do not by any means represent a complete search for different minima in χ^2 . A more elaborate analysis and, probably, more accurate data will be required to give a definitive result.

ACKNOWLEDGMENTS

We would like to thank the 30-in. bubble chamber group for their help with the exposure, and the Columbia

group for their work with the beam. We are indebted to the analysis teams at Pisa and BNL for their work. The Pisa group would like to thank Centro Studi Calcolatrici Elettroniche and Centro Nazionale Universitario di Calcolo Elettronico. We thank Dr. Philip Connolly, Dr. David Stonehill, Dr. Bernard Thevenet, and Dr. Francesco Pagni for their assistance in earlier phases of this work. Dr. C. Alff-Steinberger designed the separated beam used.

Study of Neutral Final States Produced in $\pi^- p$ Collisions at Momenta of 1.71–2.46 GeV/c

A. S. CARROLL*

Rutherford High Energy Laboratory, Chilton, Berkshire, England

AND

I. F. CORBETT, C. J. S. DAMERELL,† N. MIDDLEMAS, D. NEWTON,‡
A. B. CLEGG,‡ AND W. S. C. WILLIAMS

Nuclear Physics Laboratory, Oxford, England

(Received 24 June 1968)

We have studied neutral final states produced in $\pi^- p$ collisions at momenta of 1.71, 1.89, 2.07, 2.27, and 2.46 GeV/c, by observing the γ rays emitted. In particular, measurements are presented of (i) $\pi^- p \rightarrow \pi^0 n$, for which the Regge-pole fit at momenta ≥ 5.9 GeV/c also agrees rather well here; (ii) $\pi^- p \rightarrow \eta^0 n$, for which the Regge model which fits at higher energies does not agree here; (iii) $\pi^- p \rightarrow \pi^0 \gamma n$, in which there is some evidence for a diffraction dissociation process as well as ω^0 -meson production; (iv) $\pi^- p \rightarrow \pi^0 \pi^0 n$, which is dominated by production of $N^{*0}(1236)\pi^0$ and by peripheral production of pion pairs. In (iv), the former process is found to fit with the same Reggeized ρ -meson exchange model as charge-exchange scattering, while the latter gives indication of the s -wave $\pi\pi$ interaction. An account is given of new techniques, particularly in the data analysis, which were developed in the course of this work.

1. INTRODUCTION

THE results of a spark-chamber experiment which studied the neutral final states produced in $\pi^- p$ collisions are reported by us. When a counter system showed that an incident pion disappeared, with no outgoing charged particles produced, spark chambers surrounding the target were triggered to detect γ rays produced. The experiment was initially designed to study charge-exchange scattering,

$$\pi^- + p \rightarrow \pi^0 + n, \quad (1)$$

in the neighborhood of the $N^*(2190)$ which was reported as a peak in the $\pi^- p$ total cross sections.¹ However, it proved necessary to design the experiment so that it could also study reactions in which more than

two γ rays are produced, and other interesting results have been obtained from study of these channels.

Some of the results of this work have been published previously. In a letter² we presented graphs of the angular distributions for charge-exchange scattering, demonstrating that they were very close to the angular distributions deduced from a Regge model using the same parameters as were found to fit the angular distributions at higher momenta from 5.9 to 18.2 GeV/c. It is of course surprising that the Regge model should work at all well at the momenta of our experiment. We also showed² that the same Regge model fitted well the angular distribution found for the reaction

$$\pi^- + p \rightarrow \pi^0 + [N^{*0}(1238)] \rightarrow n + \pi^0 \quad (2)$$

in our experiment. The fit to the charge-exchange angular distributions was not perfect, but the discrepancy was such as could be explained by interference

* Present address: Brookhaven National Laboratory, Upton, N. Y.

† Present address: Rutherford High Energy Laboratory, Chilton, Berkshire, England.

‡ Present address: University of Lancaster, Lancaster, England.
¹ A. N. Diddens, E. W. Jenkins, T. F. Kycia, and K. F. Riley, Phys. Rev. Letters **10**, 262 (1963).

² A. S. Carroll, I. F. Corbett, C. J. S. Damerell, N. Middlemas, D. Newton, A. B. Clegg, and W. S. C. Williams, Phys. Rev. Letters **16**, 288 (1966); **17**, 1274(E) (1966).